

Article

The Normal Casimir Force for Lateral Moving Planes with Isotropic Conductivities

Nail Khusnutdinov *  and Natalia Emelianova

Centro de Matemática, Computação e Cognição, Universidade Federal do ABC, Santo André 09210-170, SP, Brazil; natalia7emelianova@gmail.com

* Correspondence: nail.khusnutdinov@gmail.com

Abstract: We consider the two planes at zero temperature with isotropic conductivity that are in relative lateral motion with velocity v and interplane distance a . Two models of conductivity are taken into account—the constant and frequency-dependent Drude models. The normal (perpendicular to planes) Casimir force is analyzed in detail for two systems—(i) two planes with identical conductivity and (ii) one plane that is a perfect metal. The velocity correction to the Casimir energy, $\Delta_v \mathcal{E} \propto v^2$, for small enough velocities is used for all considered cases. In the case of constant conductivity, η , the energy correction is $\Delta_v \mathcal{E} \propto \eta/a^3 (v/\eta)^2$ for $v \ll \eta \ll 1$.

Keywords: dynamic Casimir effect; lateral motion; constant conductivity

1. Introduction

The Casimir effect was initially considered for perfect conductive plates, and has now been extended to many non-ideal and new materials [1,2]. Hendrik Casimir noted in Ref. [3] that Niels Bohr suggested considering the zero-point energy as an origin of this effect and simplifying the derivation of the force. In the case of perfect conductive planes, the Casimir effect relies solely on fundamental constants and interplane distance. However, for actual materials, the Casimir effect depends on various factors, such as the shape and structure of the material, conductivity, chemical potential, temperature, and the presence of impurities [1,2].

The Casimir force between bodies is further influenced by their relative motions (see the recent review on the dynamic Casimir effect [4] and Refs. [1,5,6]). The relative motions are lateral (parallel to the planes), perpendicular to planes, or, in general, a combination of these. The Casimir effect for perpendicularly and uniformly moving slabs was first considered in Refs. [7,8] for electromagnetic and massless scalar fields. It is a direct consequence of the quantum field theory with moving boundaries [9]. In the non-relativistic scenario, the velocity correction to the Casimir pressure is quadratic, $\propto v^2$ ($\propto v^2/c^2$ in dimensional units, where c denotes the speed of light) for both fields, but with opposite signs. For the scalar field, the relative velocity correction for Casimir pressure is $\delta \mathcal{P} = (\mathcal{P} - \mathcal{P}_{v=0})/\mathcal{P} = \frac{8}{3}v^2$, while for the electromagnetic field is $\delta \mathcal{P} = -(10/\pi^2 - 2/3)v^2$.

For the massless scalar field, $\delta \mathcal{P}$, while is negative for the electromagnetic case.

The lateral relative motion of different planes gives rise to two distinct Casimir pressures in perpendicular directions. One of these pressures acts normally to planes, similar to perpendicular motion, while the other acts along planes, known as quantum, non-contact, or Casimir friction. The study of normal force has been carried out in earlier studies [10,11] for layers in stratified dielectric media with magneto-electric and non-reciprocal constant coupling, and for plates with general electric permittivity and magnetic permeability, respectively. For a three-layer system [10], the force can be either attractive or repulsive depending on the velocity directions of the extreme layers. In the



Citation: Khusnutdinov, N.; Emelianova, N. The Normal Casimir Force for Lateral Moving Planes with Isotropic Conductivities. *Physics* **2024**, *6*, 148–163. <https://doi.org/10.3390/physics6010011>

Received: 13 November 2023

Revised: 16 December 2023

Accepted: 2 January 2024

Published: 26 January 2024



Copyright: © 2024 by the authors. Licensee MDPI, Basel, Switzerland. This article is an open access article distributed under the terms and conditions of the Creative Commons Attribution (CC BY) license (<https://creativecommons.org/licenses/by/4.0/>).

non-relativistic case, the velocity correction to the force becomes repulsive when the extreme layers have the same velocity directions with respect to the middle layer, and becomes attractive for opposite velocity directions. The velocity correction to the Casimir energy follows a similar order of magnitude, approximately proportional to v^2 . For relativistic velocities, both attractive and repulsive effects can occur. A general expression for the normal force between two plates was obtained in Ref. [11] using the Fresnel reflection coefficients. It was shown that the same quadratic correction $\propto v^2$, applies to the ordinary Casimir force.

Quantum friction is a more challenging topic for analysis and is currently a subject of debate [11–24], with some even negating its existence [11]. Two dielectric planes at different temperatures with lateral relative motion have been considered in Refs. [12,13]. The quantum friction force was calculated within the framework of Rytov fluctuation theory [25]. It was demonstrated that the force is proportional to the first power of the velocity v , but can have different signs, resulting in either the deceleration or acceleration of the planes. Mkrtchian investigated two conductive planes with relative lateral motion and calculated the force and viscosity of vacuum for different plane impedance models [14]. The dependence of the force on the interplane distance heavily relies on the chosen model, but in any case, the velocity correction to the typical Casimir force proportional v emerges as the typical dependence for Casimir friction. The quantum friction for planes with temporally dispersive conductivity was analyzed in Ref. [15], revealing a cubic, v^3 , dependence at relatively small velocities and a $v^{-1} \ln v$ -dependence at quite high velocities. In Ref. [16] a general theory for quantum friction within the framework of fluctuation electrodynamics was developed. Though Ref. [11] claims the absence of quantum friction as a whole, the existence of a normal force remains without doubt (see Ref. [17]).

The study of quantum friction using scattering theory was carried out in Refs. [18,19], demonstrating the existence of a quantum friction threshold: the friction force is zero when the relative velocity is smaller than the speed of light within the slabs' materials. The origin of quantum friction was connected to quantum Cherenkov radiation: the super-luminally moving object spontaneously emits photons. This concept is closely related to super-radiance, where a rotating body amplifies incident waves [26]. In Refs. [20,21], quantum friction was calculated for two graphene sheets using the effective action approach, revealing a velocity threshold: the friction is zero when the relative velocity is smaller than the Fermi velocity. The correlation of threshold with the findings of Refs. [18,19] arises from the feature that the Dirac electron in graphene is described by the Dirac equation with the Fermi velocity instead of the speed of light. The threshold was confirmed through different calculations in Ref. [24]. The nonperturbative approach was employed to study quantum friction in Ref. [22], where the friction force was associated with electromagnetic instability: the kinetic energy of the relative motion transforms into exponentially growing coherent radiation.

In this study, we investigate the normal force between two laterally moving planes with isotropic conductivities. Previously [24], a general approach was developed for two conductive planes with relative lateral motion, which allowed for the calculation of both normal and tangential forces. The normal force was found to reduce to the typical Casimir force for planes with tensorial conductivities [27], with a specific form for the tensor of the moving plane being used. Quantum friction was also found to arise as an imaginary part of the energy calculated for complex frequencies, as discussed in the earlier papers [28–30].

In the current paper, we focus specifically on the normal force for laterally moving planes with isotropic conductivities. As noted in the earlier studies [31,32], Ohm's law for the moving plane needs to be considered carefully. The Lorentz transformation for a moving plane with scalar constant conductivity is not straightforward, as it involves a coefficient between three vectors of the electric current and an electric field. The transformation law of the conductivity tensor was discussed previously in Ref. [32] utilizing a linear response tensor [33]. In the case of graphene, the linear response tensor plays the role of polarization tensor [24,34]. To obtain the isotropic conductivity of a moving plane,

we adopt the approach suggested in Ref. [24] for graphene and consider the formal limit where the Fermi velocity and mass gap tend to zero. In this limit, the conductivity tensor becomes isotropic in the co-moving frame of the plane. However, in the laboratory frame, the conductivity is not diagonal and depends on the velocity. It is worth noting that here we employ the graphene approach as a computational tool only. The results obtained are applicable to various compositions with isotropic conductivity, including those with temporal dispersion (not considered in Ref. [10]).

In previous studies [6,35–37], the Casimir and Casimir–Polder effects for planes with isotropic conductivity were explored. Two models of conductivity were employed: (i) the constant conductivity, $\sigma = \sigma_0 \mathbf{I}$, where σ_0 denotes the scalar constant conductivity, and \mathbf{I} is the 2×2 unit matrix, and (ii) the Drude–Lorentz model with seven oscillators $\sigma = \sigma_{\text{DL}}(\omega) \mathbf{I}$,

$$\sigma_{\text{DL}}(\omega) = \frac{f_0 \omega_p^2}{\gamma_0 - i\omega} + \sum_{j=1}^7 \frac{i\omega f_j \omega_p^2}{\omega^2 - \omega_j^2 + i\omega \gamma_j},$$

with the parameters of this model obtained from experimental data for graphite from Ref. [38]. Here, f_j, ω_j and γ_j denote parameters of the model, ω is the frequency and 0 subscript notifies the Drude contribution. The first term in the model represents a Drude-like contribution, while the other terms have a Lorentz-like form. Since graphene is a single layer of graphite, the conductivity of graphene is obtained by multiplying the above expression by the interplane distance in graphite. The estimation of the binding energy per single sheet of graphene in graphite (a stack of graphenes) made in Ref. [36] revealed that the constant conductivity model underestimates the binding energy, whereas the Drude–Lorentz seven-oscillator model aligns well with the experimental data.

Both models were employed to describe the Casimir effect in a stack of graphene layers and the Casimir–Polder effect for a micro-particle near the stack. The general case of a layered system consisting of conductive planes with tensorial conductivities was analyzed in Ref. [39]. This study demonstrated that the expressions for force and energy have the same form as those obtained for the case of scalar constant conductivity, but with corresponding reflection coefficients for transverse electric (TE) and transverse magnetic (TM) modes.

In the case of constant conductivity, the Casimir energy exhibits a $1/a^3$ -dependence for all interplane distances. However, this relationship only holds for large interplane distances in the case of graphene, where the parameter ma is much greater than one (m is mass gap). This can be straightforwardly explained by noting that in the constant conductivity model, there are no dimensional parameters other than the interplane distance. For the case of small conductivity ($\eta_{\text{gr}} = 2\pi\sigma_{\text{gr}} = 0.0114$ for graphene), the TM mode contributes linearly in η , while the TE mode contributes as η^2 . However, this is not the case for two graphenes, where both modes contribute quadratically. As previously mentioned in Ref. [24], the spatial dispersion of conductivity plays an important role in the Casimir effect, causing the contribution to change from linear to quadratic.

The paper is organized as follows. In Section 2, we re-derive the conductivity of a moving graphene sheet by applying boundary conditions and obtain the main formula for normal Casimir energy. We discuss the problem of determining the eigenvalues of the product of reflection matrices. The Fresnel matrices do not commute, and their eigenvalues are not simply the product of the eigenvalues of the individual reflection matrices. Additionally, we briefly discuss the general property of lateral force along the planes and demonstrate that the necessary condition for this force is that the modulus of the Fresnel matrices is greater than one, indicating the production of photons. In Section 3, we obtain the expressions for the normal Casimir force for isotropic conductivity in two scenarios: (i) two identical planes and (ii) an isotropic plane and a perfect metal. We perform numerical calculations of the Casimir energy and analytically derive the v^2 -dependence for the velocity correction to the energy and pressure. We also evaluate the Drude-like model of isotropic conductivity numerically and demonstrate that, for large distances, the

Drude-like model yields quite similar results to the constant conductivity model. Finally, in the conclusion in Section 4, we discuss the results obtained in this study.

Throughout this paper, the natural units with $\hbar = c = 1$ are used; here, \hbar represents the reduced Planck’s constant.

2. The Casimir Energy of Moving Planes

We use the approach for the Casimir effect of lateral moving graphene developed in Ref. [24] as a computational trick. In order to provide a comprehensive understanding of this approach, let us review the key steps of derivations of the normal force outlined in Ref. [24] with some expanded explanations.

The system under consideration involves two parallel conductive planes with isotropic conductivities and an interplane distance, a . The first plane remains stationary in the laboratory frame, while the second plane undergoes lateral motion with a velocity v . The fluctuating electric field induces a current in the second plane following Ohm’s law. This current affects the boundary condition and ultimately alters the energy spectrum. The current induced in the second conductive plane, which is in motion, is described by Ohm’s law in its co-moving frame. To solve the scattering problem in the laboratory frame, it is necessary to determine the conductivity of the second plane in laboratory frame. The Lorentz transformation of Ohm’s law was discussed in Ref. [31,32]. Given that Ohm’s law has no covariant form, as it represents a linear relationship between the three-vector of the electric field and current density, the method of linear response tensor, $\Pi^{\mu\nu}$ [33], is preferred in this particular case. Within the framework of this approach, the four-vector, J^μ , of the current density and the four-potential, A^ν , are linearly connected through a tensor of linear response: $J^\mu = \Pi^\mu_\nu A^\nu$. Here, the Greek letter indices denote the time (0) and space (1, 2, 3) coordinates, x^μ , under the space-time metric (+, −, −, −). The latter represents a covariant relation that can be Lorentz-transformed into another inertial frame. This approach was successfully implemented in Refs. [31,32], where it was demonstrated that the transformation of the conductivity tensor assumes a complex and non-standard form.

A similar methodology was applied in Ref. [24] for a graphene sheet, where the polarization tensor serves as the linear response tensor. The complete action, which includes the Dirac electron, the classical electromagnetic field, and the effective action due to fermion loop correction [34], yields the following set of Maxwell equations:

$$\partial_\mu F^{\mu\nu} = -\delta(z - a)\Pi^{\nu\alpha}A_\alpha = -4\pi J^\nu, \tag{1}$$

where $z = a$ represents the position of the graphene plane and $\Pi^{\nu\alpha}$ denotes the polarization tensor resulting from the Dirac electron fermion loop. The current density assumes the form of a boundary condition. Here, $\partial_\mu \equiv \partial/\partial x_\mu$, $F_{\mu\nu}$ represents the electromagnetic tensor, and $\delta(z - a)$ is the Dirac delta function. By integrating the relationship (1) over an infinitesimally small interval ($a - \epsilon, a + \epsilon$) with ϵ approaching zero, Equation (1) can be transformed into Ohm’s law with the conductivity tensor,

$$\sigma^{ab} = \frac{\Pi^{ab}}{i\omega},$$

where the lower-case Latin letter indices take the values 1, 2.

The invariance of the boundary conditions with respect to 3-boosts,

$$\Lambda = \begin{pmatrix} u^0 & -\mathbf{u} \\ -\mathbf{u} & \mathbf{I} + \frac{\mathbf{u} \otimes \mathbf{u}}{u^0 + 1} \end{pmatrix}, \quad \mathbf{u} = (u^1, u^2), \tag{2}$$

along the graphene plane was utilized in Ref. [24] to determine the transformation of the conductivity tensor of graphene to the laboratory frame, with u denoting the spacial velocity and \otimes representing the tensor product. In the current study, we employ this approach to calculate the boost transformation of the isotropic conductivity tensor. The conductivity tensor in the laboratory frame is represented by

$$\sigma = \frac{\omega'}{\omega} \mathbf{G} \sigma' \mathbf{G}^T, \tag{3}$$

where

$$\mathbf{G} = \mathbf{I} - \frac{\omega}{(ku)} \frac{\mathbf{u} \otimes \mathbf{u}}{u_0 + 1} + \frac{\mathbf{u} \otimes \mathbf{k}}{(ku)},$$

k represents the wave vector and the prime denotes the quantities defined in the co-moving frame.

In the framework of the scattering matrix approach [27], the Casimir energy density, \mathcal{E} , per unit area can be expressed in terms of the scattering matrix, \mathcal{S} :

$$\mathcal{E} = \frac{i}{4\pi} \iint \frac{d^2k}{(2\pi)^2} \int_0^\infty \ln \det \mathcal{S} \frac{k_3 dk_3}{\sqrt{k^2 + k_3^2}}, \tag{4}$$

where the \mathcal{S} -matrix of the total system consists of the reflection, \mathbf{R} , and transmission, \mathbf{T} , matrices:

$$\mathcal{S} = \begin{pmatrix} \mathbf{R} & \mathbf{T}' \\ \mathbf{T} & \mathbf{R}' \end{pmatrix}.$$

The matrix (2) describes the scattering of the electromagnetic field:

$$\begin{pmatrix} \overleftarrow{\mathbf{E}}_l \\ \overleftarrow{\mathbf{E}}_r \end{pmatrix} = \mathcal{S} \begin{pmatrix} \overrightarrow{\mathbf{E}}_l \\ \overrightarrow{\mathbf{E}}_r \end{pmatrix},$$

where the direction of the vector indicates the direction of the wave, $\overrightarrow{\mathbf{E}} \propto e^{+ik_3z}$, $\overleftarrow{\mathbf{E}} \propto e^{-ik_3z}$ and indexes "l" and "r" stand for electromagnetic field on the left and right sides of the total system, correspondingly. The system, in general, can consist of a set of planes. The vectors over the fields denote the wave direction. The scattering matrix \mathcal{S} cannot be reduced to a product of matrices for each plane [39].

The general relation can be transformed [27] into the following expressions for the energy density, \mathcal{E} , and the pressure, \mathcal{P} , for real frequencies:

$$\mathcal{E} = -\frac{1}{2i} \iint \frac{d^2k}{(2\pi)^3} (I_- - I_+) \quad \text{and} \quad \mathcal{P} = \iint \frac{d^2k}{(2\pi)^3} (J_- + J_+), \tag{5}$$

where

$$I_\pm = \int_k^\infty d\omega \ln \det \left[1 - e^{\pm 2iak_3} \mathcal{R}(\pm k_3) \right], \tag{6}$$

$$J_\pm = \int_k^\infty d\omega k_3 \frac{e^{\pm 2iak_3} (\text{tr} \mathcal{R}(\pm k_3) - 2e^{\pm 2iak_3} \det \mathcal{R}(\pm k_3))}{\det [\mathbf{I} - e^{\pm 2iak_3} \mathcal{R}(\pm k_3)]}, \tag{7}$$

$\mathcal{R}(\pm k_3) = r'_I(\pm k_3) r_{II}(\pm k_3)$, $k_3 = \sqrt{\omega^2 - k^2}$ and r_A with $A = I, II$ denote the reflection matrices. The integration in Equation (5) is taken over the xy -plane. Formulas (5) only consider the propagating waves, because $\omega \geq k$. The subscript $I(II)$ indicates that all reflection matrices are related to the rest (moving) plane.

The scattering matrix for each part of the system (each plane) has the following form:

$$\mathcal{S}_A = \begin{pmatrix} r_A & t'_A \\ t_A & r'_A \end{pmatrix},$$

with the corresponding index $A = I, II$ and argument. It connects the electromagnetic waves on the left side (l) of the specific plane of the system with that on the right (r) side by relation:

$$\begin{pmatrix} \overleftarrow{\mathbf{E}}_l \\ \overrightarrow{\mathbf{E}}_r \end{pmatrix} = \mathcal{S}_A \begin{pmatrix} \overrightarrow{\mathbf{E}}_l \\ \overleftarrow{\mathbf{E}}_r \end{pmatrix}.$$

The reflection matrices for the conductive plane were derived in Ref. [27] using the boundary condition on the plane:

$$r_A = r'_A = -\frac{\omega^2 \eta_A - \mathbf{k} \otimes (\mathbf{k} \eta_A) + \mathbf{I} \omega k_3 \det \eta_A}{\omega^2 \text{tr} \eta_A - \mathbf{k} \mathbf{k} \eta_A + \omega k_3 (1 + \det \eta_A)}, \tag{8}$$

where $\eta_A = 2\pi\sigma_A$, and σ_i is the conductivity tensor of the plane $A = I, II$. In domain $\omega < k$, there are evanescent and waveguide modes [40], but, as demonstrated in this Section below, through the rotation of the contour of integration to the imaginary axis, the contribution of these modes is cancelled out with the energy of the boundary states of corresponding modes.

Then, a rotation of the integration contour over the real axis, $\Re \omega$, in I_{\pm} (6) and J_{\pm} (7) is applied to the imaginary axis, $\Im \omega$; see Figure 1.

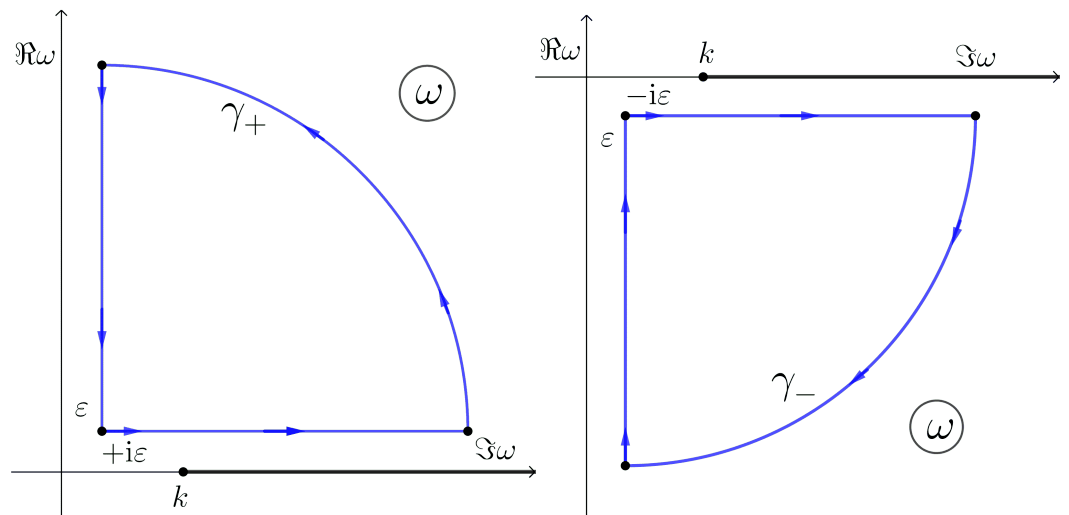


Figure 1. The contours γ_{\pm} of integration for I_{\pm} (6) and J_{\pm} (7) in the ω -plane. The integration over imaginary frequency, $\zeta = -i\omega$, yields the energy, \mathcal{E}^{\perp} . The potential presence of poles within the contours may contribute to a non-zero energy \mathcal{E}^{\parallel} . ϵ denotes an infinitely small distance to the axes and k is the wave vector.

After the rotation of the contour to the imaginary axis, two contributions survive, which we refer to as \mathcal{E}^{\perp} and \mathcal{E}_{\parallel} , corresponding to normal (real) and parallel (imaginary) to the planes, respectively. The first contribution with integration along the imaginary frequency, $\zeta = -i\omega$, is given by

$$\mathcal{E}^{\perp} = \iint \frac{d^2k}{2(2\pi)^3} \int_{-\infty}^{+\infty} d\zeta \ln \det \left[1 - e^{-2ak_E} \mathcal{R}(ik_E) \right], \tag{9}$$

where $k_E = \sqrt{\zeta^2 + k^2}$. The corresponding force is perpendicular to the planes, as is typical for the Casimir force. This expression can be simplified by using the eigenvalues of matrix \mathcal{R} and can be represented as a sum of TE and TM contributions. The matrices r'_I and r_{II} do not commute (see below in this Section), and therefore the eigenvalues of \mathcal{R} are not a product of the eigenvalues of r'_I and r_{II} . The eigenvalues of \mathcal{R} can be found in closed, albeit complicated, forms [24], corresponding to the contributions of the TM and TE modes separately. Instead of applying this approach, we use the expression for energy in the form [27] straightforwardly including the conductivity matrices, η_A :

$$\mathcal{E}^\perp = \int \frac{d^2k}{(2\pi)^3} \int_{-\infty}^\infty d\zeta \ln \left(1 + e^{-4ak_E} \frac{\zeta^2 k_E^2}{b_I b_{II}} \det \boldsymbol{\eta}_I \det \boldsymbol{\eta}_{II} - e^{-2ak_E} \left[\frac{\zeta^2 k_E^2}{b_I b_{II}} [(1 - \det \boldsymbol{\eta}_I)(1 - \det \boldsymbol{\eta}_{II}) + \det(\boldsymbol{\eta}_I - \boldsymbol{\eta}_{II})] - \frac{\zeta k_E}{b_I} - \frac{\zeta k_E}{b_{II}} + 1 \right] \right), \quad (10)$$

where $b_A = \zeta^2 \text{tr } \boldsymbol{\eta}_A + (\mathbf{k} \boldsymbol{\eta}_A \mathbf{k}) + \zeta k_E (1 + \det \boldsymbol{\eta}_A)$. The \mathcal{E}_\parallel contribution represents the Casimir friction.

If the conductivity tensor is given by

$$\boldsymbol{\eta}_A = \eta_A^{\text{TE}} \mathbf{I} + (\eta_A^{\text{TM}} - \eta_A^{\text{TE}}) \frac{\mathbf{k} \otimes \mathbf{k}}{k^2}, \quad (11)$$

it possesses the eigenvalues η_A^{TM} and η_A^{TE} , corresponding to the TM and TE modes, respectively. In particular, the graphene conductivity tensor has such a structure [34] with corresponding conductivities of modes. The Hall conductivity gives an additional antisymmetric term [41]. In this case, the expression (10) for Casimir energy can be transformed to the known [1] form of sum contributions for the TE and TM modes:

$$\mathcal{E}^\perp = \int \frac{d^2k}{(2\pi)^3} \int_{-\infty}^\infty d\zeta \left[\ln \left(1 - \frac{e^{-2ak_E}}{\left(1 + \frac{k_E}{\zeta \eta_I^{\text{TE}}}\right) \left(1 + \frac{k_E}{\zeta \eta_{II}^{\text{TE}}}\right)} \right) + \ln \left(1 - \frac{e^{-2ak_E}}{\left(1 + \frac{k_E}{\zeta \eta_I^{\text{TM}}}\right) \left(1 + \frac{k_E}{\zeta \eta_{II}^{\text{TM}}}\right)} \right) \right].$$

In the case considered here, the conductivity of the moving plane does not have form (11), and we use the Casimir energy in the form (10).

In Ref. [24], the normal force was considered for moving graphene with the following conductivity in a co-moving frame:

$$\boldsymbol{\eta} = \eta_{\text{gr}} \frac{\tilde{k}}{\omega} \left(\mathbf{I} + v_F^2 \frac{\mathbf{k} \otimes \mathbf{k}}{\tilde{k}^2} \right) \tilde{\Phi} \left(\frac{\tilde{k}}{2m} \right), \quad (12)$$

where $\eta_{\text{gr}} = \pi e^2 / 2$ with e the electron charge, v_F is the Fermi velocity,

$$\tilde{\Phi}(y) = \frac{2i}{\pi y} \left(1 - \frac{y^2 + 1}{y} \text{arctanh } y \right) \text{ and } \tilde{k} = \sqrt{\omega^2 - v_F^2 k^2}. \quad (13)$$

In the laboratory frame, the general structure of the moving plane's conductivity tensor (3) takes the form [24]

$$\boldsymbol{\eta}_{II} = i_1 \mathbf{I} + i_2 \mathbf{k} \otimes \mathbf{k} + i_3 (\mathbf{k} \otimes \mathbf{v} + \mathbf{v} \otimes \mathbf{k}), \quad (14)$$

where

$$\begin{aligned} i_1 &= \frac{\eta_{\text{gr}} \tilde{\Phi}'}{\omega k^2 \tilde{k}'} \left(k^2 \tilde{k}'^2 + \frac{1 - v_F^2}{1 - v^2} ((\mathbf{k} \mathbf{v})^2 - k^2 v^2) k_3^2 \right), \\ i_2 &= \frac{\eta_{\text{gr}} \tilde{\Phi}'}{\omega k^2 \tilde{k}'} \left(k^2 v_F^2 + \frac{1 - v_F^2}{1 - v^2} v^2 k_3^2 \right), \\ i_3 &= \frac{\eta_{\text{gr}} \tilde{\Phi}'}{k^2 \tilde{k}'} \frac{1 - v_F^2}{1 - v^2} (k^2 - \omega(\mathbf{k} \mathbf{v})), \end{aligned} \quad (15)$$

and

$$\tilde{k}' = \sqrt{\tilde{k}^2 + \frac{1 - v_F^2}{1 - v^2} [\omega^2 v^2 + (\mathbf{k}v)^2 - 2\omega(\mathbf{k}v)]}, \tag{16}$$

is the Lorentz transformation of \tilde{k} (13).

The reflection matrices r_i (8), on the basis of eigenvectors, are given as

$$\hat{r}_I(k_3) = - \begin{pmatrix} \frac{k_3 \eta}{\eta k_3 + \tilde{k}} & 0 \\ 0 & \frac{\eta \tilde{k}}{\eta \tilde{k} + k_3} \end{pmatrix} \text{ and } \hat{r}_{II}(k_3) = - \begin{pmatrix} \frac{k_3 \eta'}{\eta' k_3 + \tilde{k}'} & 0 \\ 0 & \frac{\eta' \tilde{k}'}{\eta' \tilde{k}' + k_3} \end{pmatrix}, \tag{17}$$

where the hat denotes the diagonalized reflection matrices, $\eta = \eta_{gr} \tilde{\Phi}(y)$, $\eta' = \eta_{gr} \tilde{\Phi}(y')$, and

$$\mathbf{T}_A^{-1} \mathbf{r}_A \mathbf{T}_A = \hat{\mathbf{r}}_A \Leftrightarrow \mathbf{r}_A = \mathbf{T}_A \hat{\mathbf{r}}_A \mathbf{T}_A^{-1}. \tag{18}$$

The matrices \mathbf{T}_i diagonalize the reflection matrices r_i and have the form

$$\mathbf{T}_I = \begin{pmatrix} k_2 & k_1 \\ -k_1 & k_2 \end{pmatrix} \text{ and } \mathbf{T}_{II} = \begin{pmatrix} k_2 - v_2 \frac{k_3^2}{\omega - (\mathbf{k}v)} & k_1 - v_1 \omega \\ -k_1 + v_1 \frac{k_3^2}{\omega - (\mathbf{k}v)} & k_2 - v_2 \omega \end{pmatrix}.$$

It is worth noting that the eigenvalues of r_{II} can be obtained from the eigenvalues of r_I through a Lorentz transformation. Specifically, $k_3 \rightarrow k_3$, $\tilde{k} \rightarrow \tilde{k}'$, and $\eta \rightarrow \eta'$ under these transformations, resulting in $\hat{r}_I \rightarrow \hat{r}_{II}$. This is expected, as eigenvalues are invariants of a matrix.

The eigenvector basis of r_I ,

$$\mathbf{a}_1 = (k_2, -k_1), \mathbf{a}_2 = (k_1, k_2) = \mathbf{k},$$

is orthogonal with $\mathbf{a}_1 \cdot \mathbf{a}_2 = 0$, and $\mathbf{a}_1^2 = \mathbf{a}_2^2 = \mathbf{k}^2$. On the other hand, the eigenvector basis of r_{II} ,

$$\mathbf{c}_1 = \left(k_2 - v_2 \frac{k_3^2}{\omega - (\mathbf{k}v)}, -k_1 + v_1 \frac{k_3^2}{\omega - (\mathbf{k}v)} \right),$$

$$\mathbf{c}_2 = (k_1 - v_1 \omega, k_2 - v_2 \omega),$$

is not orthogonal:

$$\mathbf{c}_1 \cdot \mathbf{c}_2 = \frac{\mathbf{k}^2 - \omega(\mathbf{k}v)}{\omega - (\mathbf{k}v)} (\mathbf{k}v n) \neq 0, \tag{19}$$

where $n^a = \delta_3^a$ with δ_b^a the Kronecker delta. Through straightforward calculations, the following expression for the commutator is obtained:

$$[\mathbf{r}_I, \mathbf{r}_{II}] = \eta \eta' \frac{(1 - v_F^2)^2}{1 - v^2} \frac{\omega((\mathbf{k}v)\omega - k^2)}{\tilde{k} \tilde{k}' b_I b_{II}} (k_3^2 \mathbf{k} \otimes \mathbf{v} - \omega^2 \mathbf{v} \otimes \mathbf{k}), \tag{20}$$

Therefore, the commutator $[\mathbf{r}_I, \mathbf{r}_{II}] \neq 0$ and the r_I and r_{II} cannot be diagonalized simultaneously; this means that the eigenvalues of $r_I \cdot r_{II}$ are not a product of the eigenvalues of the matrices r_I and r_{II} .

The straightforward calculations give the following expression for the eigenvalues of matrix \mathcal{R} :

$$r_{TM/TE}(k_3) = \frac{\eta \eta'}{2PQP'Q'} \left\{ \alpha \left(k_3 \left(k^2 Q' + Q \left((ku)^2 - k_3^2 \right) \right) + \alpha \left((ku)\omega - k_3^2 u_0 \right)^2 \right) + 2k_3^2 Q Q' \right. \\ \left. \pm \alpha \sqrt{\left(k_3 \left(k^2 Q' + Q \left((ku)^2 - k_3^2 \right) \right) + \alpha \left((ku)\omega - k_3^2 u_0 \right)^2 \right)^2 + 4k_3^4 Q Q' \left((ku)^2 - k^2 u^2 \right)} \right\}, \tag{21}$$

where $\alpha = 1 - v_F^2$, \pm defines the TM (plus sign) and TE (minus sign),

$$Q = \tilde{k}\eta + k_3, P = \tilde{k} + \eta k_3, \text{ and } Q' = \tilde{k}'\eta' + k_3, P' = \tilde{k}' + \eta'k_3.$$

In the case of zero velocity, $\mathbf{u} = \mathbf{0}$, $\hat{\mathbf{r}} = \hat{\mathbf{r}}_1^2$, is obtained, as expected. To establish the correct correspondence, the following square root sign convention is employed:

$$\sqrt{(\alpha k^2 + 2k_3 Q)^2} = \alpha k^2 + 2k_3 Q, \tag{22}$$

The eigenvalues (21) have quite a complex form. Hence, expression (10) is used where the Casimir energy is directly expressed in terms of the tensors' conductivities.

Let us briefly discuss the contribution \mathcal{E}_{\parallel} , which can contribute to the force along the planes. The contribution to the Casimir pressure takes the form

$$\begin{aligned} \mathcal{P}_{\parallel} = & \iint \frac{d^2k}{(2\pi)^3} \left\{ \oint_{\gamma_-} d\omega k_3 \frac{e^{-2iak_3} (\text{tr } \mathcal{R}(-k_3) - 2e^{-2iak_3} \det \mathcal{R}(-k_3))}{\det[\mathbf{I} - e^{-2iak_3} \mathcal{R}(-k_3)]} \right. \\ & \left. + \oint_{\gamma_+} d\omega k_3 \frac{e^{2iak_3} (\text{tr } \mathcal{R}(k_3) - 2e^{2iak_3} \det \mathcal{R}(k_3))}{\det[\mathbf{I} - e^{2iak_3} \mathcal{R}(k_3)]} \right\}, \end{aligned} \tag{23}$$

with the contours γ_{\pm} as shown in Figure 1. This expression only has a non-zero value if poles appear inside the contours, satisfying the relations

$$\det[\mathbf{I} - e^{\pm 2iak_3} \mathbf{r}'_1(\pm k_3) \mathbf{r}_2(\pm k_3)] = 0. \tag{24}$$

The relation (24), within various contexts, has been noted in the earlier studies [19,28–30,42]. If the matrix \mathcal{R} has the eigenvalues r_{TM} and r_{TE} , this relation can be separated into the two scalar relations:

$$1 - e^{\pm 2iak_3} r_{\text{TM}}(\pm k_3) = 0 \text{ and } 1 - e^{\pm 2iak_3} r_{\text{TE}}(\pm k_3) = 0, \tag{25}$$

respectively.

The solutions of the relations (25) must possess imaginary parts to contribute as residues. It can be demonstrated that solutions to these relations exist if, and only if,

$$|r_{\text{TM}}(\pm k_3)| > 1 \text{ and } |r_{\text{TE}}(\pm k_3)| > 1. \tag{26}$$

Since $\text{sign}(\Im k_3) = \text{sign}(\Im \omega)$, then

$$\left| e^{\pm 2iak_3} \right| = \left[e^{\pm 2iak_3} e^{\mp 2iak_3^*} \right]^{1/2} = e^{\mp 2a\Im k_3} = e^{-2a|\Im k_3|} < 1.$$

Given this inequality, one can obtain the inequalities (26) from the relations (25).

Then, it follows that the condition $\mathcal{P}_{\parallel} \neq 0$ is associated with virtual photon production because the modulus of the reflection coefficients is greater than 1. Lifshitz demonstrated [43] that without relative velocity, Equation (24) has no solutions since the inequalities (26) cannot be satisfied. This statement can be proven for graphene with zero mass gap (for simplicity). For velocity $v = 0$ and $m = 0$,

$$\begin{aligned} r_{\text{TM}}^{-1}(\pm k_3) &= \left(1 \pm \frac{\tilde{k}}{\eta k_3} \right)^2 = \left(1 + \frac{\tilde{k}}{\eta_{\text{gr}} k_3} \right)^2, \\ r_{\text{TE}}^{-1}(\pm k_3) &= \left(1 \pm \frac{k_3}{\eta \tilde{k}} \right)^2 = \left(1 + \frac{k_3}{\eta_{\text{gr}} \tilde{k}} \right)^2, \end{aligned} \tag{27}$$

are obtained. Then,

$$|r_{TM}^{-1}(\pm k_3)| = \left(1 + \frac{|\tilde{k}|^2}{\eta_{gr}^2 |k_3|^2} + 2 \frac{\Re \tilde{k} \Re k_3 + \Im \tilde{k} \Im k_3}{\eta_{gr} |k_3|^2} \right)^2. \tag{28}$$

It can be straightforwardly shown that $\Re \tilde{k} \Re k_3 + \Im \tilde{k} \Im k_3 > 0$, thus, satisfying

$$|r_{TM}^{-1}(\pm k_3)| > 1. \tag{29}$$

Hence, one concludes that the inequalities (26) cannot be satisfied in the case considered in this paper, indicating there are no solutions for Equation (24). However, one would expect that solutions may exist due to relative motion of the planes.

3. The Case of Isotropic Conductivity

The case of isotropic conductivity can be obtained by taking the formal limits $v_F \rightarrow 0$ and $\tilde{\Phi} \rightarrow 1$ ($m \rightarrow 0$) in Equation (12) and replacing the graphene conductivity, η_{gr} , with the conductivity, η_i , of the corresponding plane. After taking these limits, the conductivity tensor for the plane at rest becomes diagonal $\eta_I = \eta_I \mathbf{I}$ and $\tilde{k}' = \gamma \omega_v$, where $\omega_v = \omega - \mathbf{k}v$, $\gamma = 1/\sqrt{1 - v^2}$ is the relativistic factor, and

$$\eta_{II} = i'_1 \mathbf{I} + i'_2 \mathbf{k} \otimes \mathbf{k} + i'_3 (\mathbf{k} \otimes \mathbf{v} + \mathbf{v} \otimes \mathbf{k}), \tag{30}$$

where

$$i'_1 = \frac{\eta_{II} \gamma (\mathbf{k}^2 \omega_v^2 + ((\mathbf{k}v)^2 - \mathbf{k}^2 v^2) k_3^2)}{\mathbf{k}^2 \omega \omega_v}, \quad i'_2 = \frac{\eta_{II} \gamma v^2 k_3^2}{\mathbf{k}^2 \omega \omega_v}, \quad i'_3 = \frac{\eta_{II} \gamma}{\mathbf{k}^2 \omega_v} (\mathbf{k}^2 - \omega(\mathbf{k}v)). \tag{31}$$

The quantity $\omega_v \gamma$ represents the frequency of photons in a laboratory that was emitted in a co-moving frame.

By performing straightforward calculations at the imaginary axis $\omega = i\zeta$, one obtains:

$$b_I = (\eta_I \zeta + k_E)(\zeta + \eta_I k_E), \quad b_{II} = \frac{\zeta}{\gamma \zeta_v} (\eta_{II} \gamma \zeta_v + k_E)(\gamma \zeta_v + \eta_{II} k_E),$$

$$\det(\eta_I - \eta_{II}) = (\eta_I - \eta_{II})^2 + \eta_I \eta_{II} \left(\gamma v^2 \frac{k_E^2}{\zeta \zeta_v} + 2(1 - \gamma) \right), \quad \det \eta_A = \eta_A^2, \tag{32}$$

where $\zeta_v = \zeta + i\mathbf{k}v$. Then, we use the polar coordinates for \mathbf{k} in Equation (10), $\mathbf{k}v = kv \cos \varphi$ and transform the coordinates of the plane $k \in [0, \infty)$, $\zeta \in (-\infty, \infty)$ to polar coordinates $\zeta = k_E \cos \theta$, $k = k_E \sin \theta$. After these changes, the dependence of k_E only survives in the exponents. Changing $ak_E = y$, one observes that the energy depends on the interplane distance as $1/a^3$ for constant conductivities, as expected [35]. Thus, the energy and pressure have the following form ($x = \cos \theta$):

$$\mathcal{E}_{1,2}^\perp = \Re \int_0^\infty \frac{y^2 dy}{(2\pi a)^3} \int_0^1 dx \int_0^\pi d\varphi E_{1,2}, \quad \mathcal{P}_{1,2}^\perp = \frac{3}{a} \mathcal{E}_{1,2}^\perp, \tag{33}$$

where

$$E_{1,2} = \ln \left\{ 1 + e^{-4y} \frac{x^2 \eta_I^2 \eta_{II}^2}{\beta_I \beta_{II}} - e^{-2y} \left[\frac{x^2}{\beta_I \beta_{II}} \left((1 - \eta_I \eta_{II})^2 + \eta_I \eta_{II} \left(\frac{\gamma v^2}{xx_v} + 2(1 - \gamma) \right) \right) - \frac{x}{\beta_I} - \frac{x}{\beta_{II}} + 1 \right] \right\}, \tag{34}$$

and

$$\beta_I = (\eta_I x + 1)(x + \eta_I), \beta_{II} = \frac{x}{\gamma x_v} (\eta_{II} \gamma x_v + 1)(\gamma x_v + \eta_{II}), x_v = x + i v \sqrt{1 - x^2} \cos \varphi. \tag{35}$$

If the first plane (at rest) is a perfect (ideal) conductor, one takes the limit $\eta_1 \rightarrow \infty$ and obtains

$$E_{id,2} = \ln \left[1 + e^{-4y} \frac{x \eta_{II}^2}{\beta_{II}} - e^{-2y} \left(\frac{x \eta_{II}^2}{\beta_{II}} - \frac{x}{\beta_{II}} + 1 \right) \right], \tag{36}$$

whereas for two ideal planes,

$$E_{id,id} = 2 \ln \left(1 + e^{-2y} \right), \tag{37}$$

the energy does not depend on the velocity.

The expressions (33) and (34) coincide with those obtained in Ref. [11], where two planes of finite thickness with relative lateral motion were considered. As noted in Ref. [44], the typical reflection coefficients cannot be used for 2D (two-dimensional) materials due to the impossibility of taking the limit of zero thickness. The reflection coefficients in this case have to be calculated using scattering theory [45] or 2D quantum electrodynamics[34]. In the case under consideration here, one needs to use the reflection coefficients (27) for the plane at rest and the same expressions, but with a boosted wave vector (16), for the moving plane. Then, one takes limit $v_F \rightarrow 0$ to obtain the isotropic conductivity. Finally, one arrives at Equations (33) and (34). For example, the coefficient at e^{-4y} in Equation (34) reads

$$\frac{x^2 \eta_I^2 \eta_{II}^2}{\beta_I \beta_{II}} = r_{E1} r_{E2} r_{B1} r_{B2}$$

in the notations of Ref. [11].

Without a relative movement, $v = 0$, the results obtained in Ref. [35] are reproduced:

$$E = \ln \left(1 - e^{-2y} \frac{\eta_I \eta_{II}}{(\eta_I + x)(\eta_{II} + x)} \right) + \ln \left(1 - e^{-2y} \frac{\eta_I \eta_{II} x^2}{(x \eta_I + 1)(x \eta_{II} + 1)} \right) = E_{TM} + E_{TE}, \tag{38}$$

the sum of TM and TE contributions.

Let us consider the constant conductivities case with equal conductivities: $\eta_I = \eta_{II} = \eta = \text{const}$. For $v = 0$, one obtains from Equation (33) the sum of the TM and TE mode contributions,

$$\begin{aligned} E_{1,2}^0 &= \ln \left(1 - e^{-2y} \frac{\eta^2}{(x + \eta)^2} \right) + \ln \left(1 - e^{-2y} \frac{x^2 \eta^2}{(1 + x \eta)^2} \right), \\ E_{id,2}^0 &= \ln \left(1 - e^{-2y} \frac{\eta}{x + \eta} \right) + \ln \left(1 - e^{-2y} \frac{x \eta}{1 + x \eta} \right), \end{aligned} \tag{39}$$

respectively.

In the case with $\eta \ll 1$, the Casimir energies read for $v = 0$:

$$\begin{aligned} \mathcal{E}_{1,2}^0 &= \frac{\eta}{a^3} \frac{180 \zeta_R(3) + \pi^4 + 60 \pi^2 - 1440 \ln 2}{2880 \pi^2} = -3.2 \times 10^{-3} \frac{\eta}{a^3}, \\ \mathcal{E}_{id,2}^0 &= \frac{\eta}{a^3} \left[\frac{\ln \eta}{32 \pi^2} + \frac{90 \zeta_R(3) + \pi^4 + 15 \pi^2 - 405}{2880 \pi^2} \right] = - \left[3.1 \ln \eta^{-1} + 1.8 \right] \times 10^{-3} \frac{\eta}{a^3}. \end{aligned} \tag{40}$$

To move to the dimensional SI (International System) units, one has to multiply the relations (39) and (40) by $\hbar c = 3.16 \times 10^{-26} \text{ J} \cdot \text{m}$.

For small velocity and conductivity, specifically if $v \ll \eta \ll 1$, one obtains Equation (33):

$$\frac{\Delta_v \mathcal{E}_{1,2}^\perp}{\mathcal{E}_{1,2}^0} = \frac{\Delta_v \mathcal{P}_{1,2}^\perp}{\mathcal{P}_{1,2}^0} \approx -0.19 \left(\frac{v}{\eta}\right)^2, \quad \frac{\Delta_v \mathcal{E}_{id,2}^\perp}{\mathcal{E}_{id,2}^0} = \frac{\Delta_v \mathcal{P}_{id,2}^\perp}{\mathcal{P}_{id,2}^0} \approx -\frac{0.3}{\ln \eta^{-1} + 0.57} \left(\frac{v}{\eta}\right)^2, \quad (41)$$

where $\Delta_v \mathcal{E}_{i,k}^\perp = \mathcal{E}_{i,k}^\perp - \mathcal{E}_{i,k}^0$. The relative velocity correction is quadratic in the velocity and is negative, meaning the force is decreased due to the motion of the planes.

Numerical evaluations of Equation (33) are shown in Figure 2 for two systems: (1,2)—two conductive planes with constant conductivity η (solid lines) and (id,2)—the first plane at rest, which is a perfect metal (dashed lines). We calculated the velocity correction to the energy: $\Delta_v \mathcal{E}_\perp / \mathcal{E}_0 = (\mathcal{E}_\perp - \mathcal{E}_0) / \mathcal{E}_0$, where \mathcal{E}_0 is the energy without relative movement. The velocity correction is negative for both systems and exhibits quadratic behavior, proportional to v^2 , for small velocities, $v \ll \eta \ll 1$. The absolute value of the correction is larger for the first system.

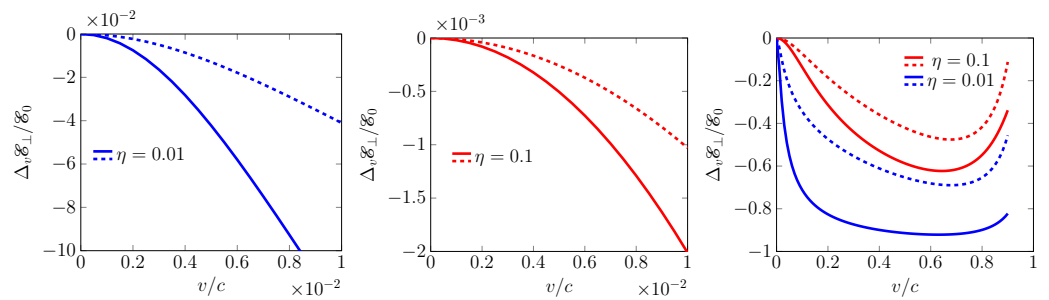


Figure 2. The velocity correction $\Delta_v \mathcal{E}_\perp / \mathcal{E}_0 = (\mathcal{E}_\perp - \mathcal{E}_0) / \mathcal{E}_0$ for $\eta = 0.01, 0.1$. In the case of small velocity and conductivity, $v \ll \eta \ll 1$ (left and middle), a quadratic correction is observed in accordance with Equation (41). The right plot shows the correction for all possible velocities. The solid lines represent two planes with equal conductivity, as given by Equation (34), while the dashed lines represent systems where one plane is stationary with perfect conductivity (described by Equation (36)), and the second plane possesses isotropic conductivity (described by Equation (34)). Here, c denotes the speed of light.

The above derivation is applicable for isotropic, but frequency-dependent (temporal dispersion), conductivity, $\eta = \eta(\omega)$. Let us consider the simple enough case of Drude-like conductivity with

$$\eta_1 = \frac{\eta \Gamma}{\Gamma + \xi}, \quad \eta_2 = \frac{\eta \Gamma}{\Gamma + \gamma \xi v}, \quad (42)$$

where parameters are considered for graphene: $\Gamma = 6.365$ eV and $\eta = \eta_{gr} = e^2/4$, where Γ denotes a scattering parameter [36]. After changing the integrand variables as in Equation (33) the Casimir energy acquires an additional dependence on the interplane distance through conductivity:

$$\eta_I = \frac{\eta_{gr}(a\Gamma)}{(a\Gamma) + yx}, \quad \eta_{II} = \frac{\eta_{gr}(a\Gamma)}{(a\Gamma) + \gamma yxv}. \quad (43)$$

For $a = 100$ nm and $\Gamma = 6.365$ eV, one has $a\Gamma = 3.225$. For large values of $a\Gamma \gg 1$, the conductivities $\eta_I = \eta_{II} = \eta_{gr}$, consistent with the constant conductivity model, are valid for large interplane distances.

The Casimir energy is numerically evaluated and presented in Figure 3. It can be observed that as the interplane distance increases, the energy approaches that of the constant conductivity case (blue lines), as expected.

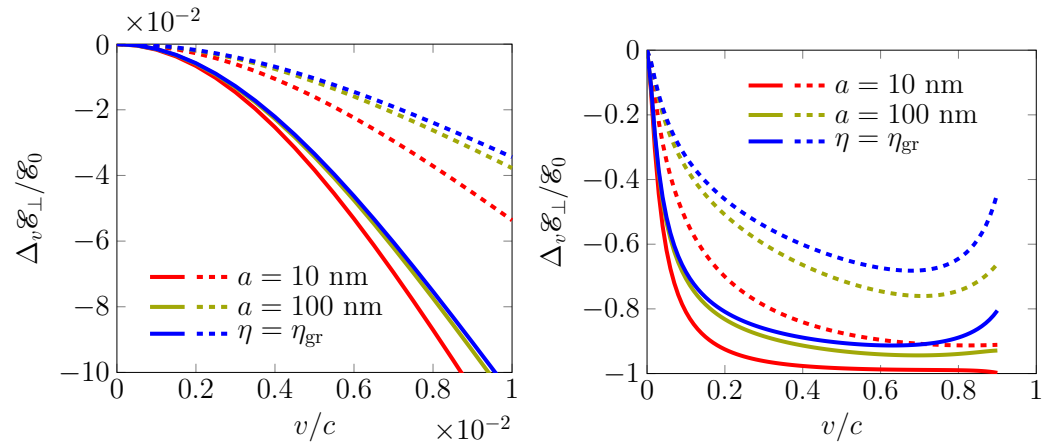


Figure 3. The velocity correction $\Delta_v \epsilon_{\perp} / \epsilon_0 = (\epsilon_{\perp} - \epsilon_0) / \epsilon_0$ for the Drude model with the parameters of the interplane distance, $a = 10$ nm and 100 nm, and constant conductivity, $\eta = \eta_{gr}$, the graphene conductivity, for small velocities, $v \ll 1$ (left), and the entire range of v (right). The solid lines correspond to two planes with equal conductivity, and the dashed lines represent a scenario where one plane is stationary with perfect conductivity. It is worth noting that as the interplane distance increases, the curves approach the scenario of constant conductivity.

To compare the results obtained here with the analysis of graphene in Ref. [24], let us consider the case of two graphene sheets. The energy initially increases with velocity and then becomes negative, reaching a maximum at $v_c = v_F + (ma)/2$. When $m = v_F = 0$, the region with positive energy disappears. Conversely, for two planes with constant conductivity, the energy is always negative for all values of velocity. Both cases exhibit a velocity correction of v^2 order. Regarding the interplane distance, different behaviors are observed. For two planes with constant conductivity, the energy has the $1/a^3$ -dependence for any a distance, while for graphene, this dependence is only evident for large distances. This is expected, as the constant conductivity model for graphene is valid for large interplane distances. In the case of a system consisting of a perfect conductor and graphene, the energy is zero up to a specific velocity, while in the aforementioned scenario, a quadratic behavior is observed at the beginning. The same conclusion holds for the Drude model of conductivity (42). For large interplane distances, both models closely align, while for small distances, a weak dependence on distance is observed.

4. Conclusions

In this paper, we investigated the normal (perpendicular to the planes) Casimir force between two conductive planes with an isotropic conductivity that moves laterally with a relative velocity v . Within the framework of scattering theory, the main challenge lies in determining the conductivity of a moving plane in a laboratory frame. In a co-moving frame, the isotropic conductivity is represented by a coefficient in Ohm’s law, $J' = \sigma' E'$, where E' and J' denote fluctuations in the electric field and corresponding current density. Transforming this relation to the laboratory frame, where the first plane is at rest, is not a trivial task. A simplified approach [31,32] to address this issue is to start from the linear relation between current density and electromagnetic vector potential, $J^{\mu} = \Pi_v^{\mu} A^{\nu}$, which is commonly used in plasma physics [33]. A similar approach was employed in Ref. [34], where the polarization tensor served as the linear response tensor Π_v^{μ} .

Even in the case of constant conductivity, the transformation of conductivity does not have quite a simple form [32]. A similar methodology was applied in Ref. [24], where the linear relations for current and electromagnetic potential, as well as the conservation of boundary conditions, were utilized. To obtain isotropic conductivity, we adapted the expressions derived for graphene, taking the limits $v_F \rightarrow 0$ for Fermi velocity and $m \rightarrow 0$ for mass gap. With these limits, the conductivity tensor in the co-moving frame becomes

diagonal. In the laboratory frame, it has the form (30). Using these tensors, the Casimir energy can be calculated using expression (10), originally derived in Ref. [27].

The expressions (34) obtained for two conductive planes and for the system (perfect conductivity)/(constant conductivity) involve two small dimensionless parameters: the velocity v of the plane and the conductivity $\eta = 2\pi\sigma$ (dimensionless for 2D systems). In the case where $v \ll \eta \ll 1$, the relative energy correction due to velocity is approximately given by the $(v/\eta)^2$ behaviour (41). This quadratic v -dependence is typical for normal force and different directions of motion [7,8,10,24]. The energy dependence on the interplane distance is $1/a^3$ for any distance, which is typical for the constant conductivity case [35], as the constant conductivity model is valid for large distances where the Casimir regime is satisfied. The Drude model of conductivity shows similar behavior of the system with a weak dependence on the interplane distances (see Figure 3).

The constant conductivity model, discussed in Refs. [6,35–37], quite well describes the Casimir effect for graphenes. However, in the case of the normal force considered in this paper, there is a significant qualitative difference. When the mass gap $m \neq 0$, the velocity correction is positive up to its maximum value of $v = v_F + am/2$, whereas the constant conductivity model gives a negative correction. As stated in Ref. [24], spatial dispersion plays a crucial role in the Casimir effect. For low conductivity values, the Casimir effect exhibits a linear dependence on conductivity in the constant conductivity case, whereas it becomes quadratic when the spatial dispersion of conductivity is taken into account.

Our future investigation concerns the quantum friction in the case of constant and isotropic conductivity. It is anticipated that the magnitude of the friction force is smaller by orders of magnitude [16] compared to the normal force. Nevertheless, the study is of importance due to quite a wide range of the different results obtained for quantum friction.

Author Contributions: Investigation: N.K. and N.E.; Writing—original draft: N.K. and N.E.; Writing—review & editing: N.K. and N.E. All authors have read and agreed to the published version of the manuscript.

Funding: N.K. was supported in part by the grants 2022/08771-5 and 2021/10128-0 from the São Paulo Research Foundation (FAPESP).

Data Availability Statement: The data are available upon reasonable request.

Conflicts of Interest: The authors declare no conflicts of interest.

References

- Bordag, M.; Klimchitskaya, G.L.; Mohideen, U.; Mostepanenko, V.M. *Advances in the Casimir Effect*; Oxford University Press: Oxford, UK, 2009; p. 768. [CrossRef]
- Woods, L.M.; Dalvit, D.A.R.; Tkatchenko, A.; Rodriguez-Lopez, P.; Rodriguez, A.W.; Podgornik, R. Materials Perspective on Casimir and van der Waals Interactions. *Rev. Mod. Phys.* **2016**, *88*, 045003. [CrossRef]
- Casimir, H.B.G. Some Remarks on the History of the so called Casimir Effect. In *Casimir Effect 50 Years Later*; Bordag, M., Ed.; World Scientific Publishing Co.: Singapore, 1998; pp. 3–9. [CrossRef]
- Dodonov, V. Fifty Years of the Dynamical Casimir Effect. *Physics* **2020**, *2*, 67–104. [CrossRef]
- Bordag, M.; Mohideen, U.; Mostepanenko, V.M. New Developments in the Casimir Effect. *Phys. Rep.* **2001**, *353*, 1–205. [CrossRef]
- Khusnutdinov, N.; Woods, L.M. Casimir Effects in 2D Dirac Materials (Scientific Summary). *JETP Lett.* **2019**, *110*, 183–192. [CrossRef]
- Bordag, M.; Petrov, G.; Robaschik, D. Calculation of the Casimir Effect for Scalar Fields with the Simplest Nonstationary Boundary Conditions. *Sov. J. Nucl. Phys.* **1984**, *39*, 828–831. Available online: <https://lib-extopc.kek.jp/preprints/PDF/1983/8308/8308199.pdf> (accessed on 30 December 2023). (In Russian)
- Bordag, M.; Dittes, F.-M.; Robaschik, D. Casimir Effect With Uniformly Moving Mirrors. *Sov. J. Nucl. Phys.* **1986**, *43*, 1034–1038. Available online: <https://lib-extopc.kek.jp/preprints/PDF/1985/8508/8508324.pdf> (accessed on 30 December 2023).
- Fulling, S.A.; Davies, P.C.W. Radiation from a Moving Mirror in Two Dimensional Space-Time: Conformal Anomaly. *Proc. R. Soc. Lond. A* **1976**, *348*, 393–414. [CrossRef]
- Maslovski, S.I. Casimir Repulsion in Moving Media. *Phys. Rev. A* **2011**, *84*, 22506. [CrossRef]
- Philbin, T.G.; Leonhardt, U. No Quantum Friction between Uniformly Moving Plates. *New J. Phys.* **2009**, *11*, 33035. [CrossRef]
- Polevoi, V.G. Tangential Molecular Forces Caused between Moving Bodies by a Fluctuating Electromagnetic Field. *Sov. Phys. JETP* **1990**, *71*, 1119–1124. Available online: <http://jetp.ras.ru/cgi-bin/e/index/e/71/6/p1119?a=list> (accessed on 30 December 2023).

13. Dedkov, G.V.; Kyasov, A.A. Friction and Radiative Heat Exchange in a System of Two Parallel Plates Moving Sideways: Levin–Polevoi–Rytov Theory Revisited. *Chin. J. Phys.* **2018**, *56*, 3002–3011. [[CrossRef](#)]
14. Mkrtchian, V.E. Interaction between Moving Macroscopic Bodies: Viscosity of the Electromagnetic Vacuum. *Phys. Lett. A* **1995**, *207*, 299–302. [[CrossRef](#)]
15. Pendry, J.B. Shearing the Vacuum - Quantum Friction. *J. Phys. Condens. Matter* **1997**, *9*, 10301–10320. [[CrossRef](#)]
16. Volokitin, A.I.; Persson, B.N.J. Near-Field Radiative Heat Transfer and Noncontact Friction. *Rev. Mod. Phys.* **2007**, *79*, 1291–1329. [[CrossRef](#)]
17. Pendry, J.B. Quantum Friction—Fact or Fiction? *New J. Phys.* **2010**, *12*, 33028. [[CrossRef](#)]
18. Maghrebi, M.F.; Golestanian, R.; Kardar, M. Scattering Approach to the Dynamical Casimir Effect. *Phys. Rev. D* **2013**, *87*, 25016. [[CrossRef](#)]
19. Maghrebi, M.F.; Golestanian, R.; Kardar, M. Quantum Cherenkov Radiation and Noncontact Friction. *Phys. Rev. A* **2013**, *88*, 42509. [[CrossRef](#)]
20. Belén Farias, M.; Fosco, C.D.; Lombardo, F.C.; Mazzitelli, F.D. Quantum Friction between Graphene Sheets. *Phys. Rev. D* **2017**, *95*, 65012. [[CrossRef](#)]
21. Belén Farias, M.; Kort-Kamp, W.J.M.; Dalvit, D.A.R. Quantum Friction in Two-Dimensional Topological Materials. *Phys. Rev. B* **2018**, *97*, 161407. [[CrossRef](#)]
22. Brevik, I.; Shapiro, B.; Silveirinha, M.G. Fluctuational Electrodynamics in and out of Equilibrium. *Int. J. Mod. Phys. A* **2022**, *37*, 22410123. [[CrossRef](#)]
23. Guo, X.; Milton, K.A.; Kennedy, G.; Pourtolami, N. Quantum Friction in the Presence of a Perfectly Conducting Plate. *Phys. Rev. A* **2023**, *107*, 62812. [[CrossRef](#)]
24. Antezza, M.; Emelianova, N.; Khusnutdinov, N. Casimir-Lifshitz Force for Moving Graphene. *arXiv* **2023**, arXiv:2303.03115. <https://doi.org/10.48550/arXiv.2303.03115>.
25. Levin, M.L.; Rytov, S.M. *Theory of Equilibrium Thermal Fluctuations in Electrodynamics*; Nauka: Moscow, Russia, 1967. (In Russian)
26. Zel'dovich, Y.B. Generation of Waves by a Rotating Body. *JETP Lett.* **1971**, *14*, 270–272. Available online: http://jetpletters.ru/ps/1604/article_24607.shtml (accessed on 30 December 2023).
27. Fialkovsky, I.; Khusnutdinov, N.; Vassilevich, D. Quest for Casimir Repulsion between Chern-Simons Surfaces. *Phys. Rev. B* **2018**, *97*, 165432. [[CrossRef](#)]
28. Van Kampen, N.G.; Nijboer, B.N.A.; Schram, K. On the Macroscopic Theory of van der Waals Forces. *Phys. Lett. A* **1968**, *26*, 307–308. [[CrossRef](#)]
29. Gerlach, E. Equivalence of van der Waals Forces between Solids and the Surface–Plasmon Interaction. *Phys. Rev. B* **1971**, *4*, 393–396. [[CrossRef](#)]
30. Silveirinha, M.G. Optical Instabilities and Spontaneous Light Emission by Polarizable Moving Matter. *Phys. Rev. X* **2014**, *4*, 31013. [[CrossRef](#)]
31. Starke, R.; Schober, G.A.H. Functional Approach to Electrodynamics of Media. *Photonics Nanostruct. Fundam. Appl.* **2015**, *14*, 1–34. [[CrossRef](#)]
32. Starke, R.; Schober, G.A.H. Relativistic Covariance of Ohm’s Law. *Int. J. Mod. Phys. D* **2016**, *25*, 1640010. [[CrossRef](#)]
33. Melrose, D.B. *Quantum Plasmadynamics: Unmagnetized Plasmas*; Springer: New York, NY, USA, 2008. [[CrossRef](#)]
34. Bordag, M.; Fialkovsky, I.V.; Gitman, D.M.; Vassilevich, D.V. Casimir Interaction between a Perfect Conductor and Graphene Described by the Dirac Model. *Phys. Rev. B* **2009**, *80*, 245406. [[CrossRef](#)]
35. Khusnutdinov, N.; Drosdoff, D.; Woods, L.M. Casimir Energy for Surfaces with Constant Conductivity. *Phys. Rev. D* **2014**, *89*, 85033. [[CrossRef](#)]
36. Khusnutdinov, N.; Kashapov, R.; Woods, L.M. Casimir Effect for a Stack of Conductive Planes. *Phys. Rev. D* **2015**, *92*, 45002. [[CrossRef](#)]
37. Khusnutdinov, N.; Kashapov, R.; Woods, L.M. Casimir-Polder Effect for a Stack of Conductive Planes. *Phys. Rev. A* **2016**, *94*, 12513. [[CrossRef](#)]
38. Djurišić, A.B.; Li, E.H. Optical Properties of Graphite. *J. Appl. Phys.* **1999**, *85*, 7404–7410. [[CrossRef](#)]
39. Emelianova, N.; Khusnutdinov, N.; Kashapov, R. Casimir Effect for a Stack of Graphene Sheets. *Phys. Rev. B* **2023**, *107*, 235405. [[CrossRef](#)]
40. Bordag, M. Electromagnetic Vacuum Energy for Two Parallel Slabs in Terms of Surface, Waveguide, and Photonic Modes. *Phys. Rev. D* **2012**, *85*, 25005. [[CrossRef](#)]
41. Antezza, M.; Fialkovsky, I.; Khusnutdinov, N. Casimir-Polder Force and Torque for Anisotropic Molecules Close to Conducting Planes and Their Effect on CO₂. *Phys. Rev. B* **2020**, *102*, 195422. [[CrossRef](#)]
42. Henkel, C.; Joulain, K.; Mulet, J.P.; Greffet, J.J. Coupled Surface Polaritons and the Casimir Force. *Phys. Rev. A* **2004**, *69*, 23808. [[CrossRef](#)]
43. Lifshitz, E.M. The Theory of Molecular Attractive Forces between Solids. *Sov. Phys. JETP* **1956**, *2*, 73–83. Available online: <http://jetp.ras.ru/cgi-bin/e/index/e/2/1/p73?a=list> (accessed on 30 December 2023).

44. Bordag, M.; Geyer, B.; Klimchitskaya, G.L.; Mostepanenko, V.M. Lifshitz-Type Formulas for Graphene and Single-Wall Carbon Nanotubes: van der Waals and Casimir Interactions. *Phys. Rev. B* **2006**, *74*, 205431. [[CrossRef](#)]
45. Jaekel, M.T.; Reynaud, S. Casimir Force between Partially Transmitting Mirrors. *J. Phys. Fr.* **1991**, *1*, 1395–1409. [[CrossRef](#)]

Disclaimer/Publisher’s Note: The statements, opinions and data contained in all publications are solely those of the individual author(s) and contributor(s) and not of MDPI and/or the editor(s). MDPI and/or the editor(s) disclaim responsibility for any injury to people or property resulting from any ideas, methods, instructions or products referred to in the content.